Charnia-like broadband plasmonic nano-antenna

Ziyuan Li [a], Haroldo T. Hattori [a] & Evgeny G. Mironov [a]

[a] School of Engineering and Information Technology, University of New South Wales, Canberra, Australia
Published online: 01 Jul 2013.

PLEASE SCROLL DOWN FOR ARTICLE

Taylor & Francis
Taylor & Francis Group

Charnia-like broadband plasmonic nano-antenna

Ziyuan Li, Haroldo T. Hattori* and Evgeny G. Mironov

School of Engineering and Information Technology, University of New South Wales, Canberra, Australia

Charnia was a pre-Cambrian life-form that exhibited a fractal structure to improve the extraction of nutrients from the pre-historic seas. Inspired by its fractal structure, this paper studies the potential application of these self-similarity fractal structures to create a plasmonic nano-antenna that can operate over a large linewidth. These devices are studied both theoretically and experimentally. It is shown that these nano-antennas can produce electric field enhancements above 8 over 200 nm range and surface enhanced Raman scattering (SERS) enhancements higher than 10^5.

Keywords: integrated optics; surface plasmons; surface enhanced Raman scattering; plasmonic nano-antenna

1. Introduction

Inspired by radio wave antennas, nano-antennas working at visible and near-infrared frequencies are emerging in physical optics. They are designed to efficiently convert free-propagating optical radiation into localized energy by exploiting the unique properties of metal nanostructures that behave as strongly coupled plasmas at optical frequencies [1,2]. Moreover, the advent of novel top-down nanofabrication tools (e.g. focused ion beam milling and electron-beam lithography) and bottom-up self-assembly schemes introduced the possibility of fabricating them with small footprints in the order of a wavelength of light. Therefore, these devices can be used to manipulate, control, and visualize optical fields on a nanometric scale that surpasses conventional diffraction limit.

Currently, studies of plasmonic nano-antennas, which are constructed by placing a sub-wavelength dielectric (e.g. air) gap between two metallic regions, have attracted considerable interest. This is mainly due to the fact that the hot spots (regions of intense and localized electric fields) in nano-antennas produce highly intense electromagnetic fields in sub-wavelength areas. It is found that dipole and bowtie antennas can confine fields in nano-scale volumes at several orders of magnitude below the wavelength limit defined by the gap dimensions [3,4]. Moreover, they can enhance the incident electric field near the surface of the metallic region by several orders of magnitude and produce enhancement factors as high as a hundred [5]. These localized high-intensity electric fields can be used to excite nonlinear effects, such as surface enhanced Raman scattering (SERS), to visualize and manipulate nanoparticles and reduce divergences of semiconductor lasers.

Although plasmonic nano-antennas have been used in many applications, their usually narrow-band spectra with sharp resonances are a major challenge for applications that require devices operating over a wide range of frequencies. For example, when nano-antennas are utilized in solar cells as electromagnetic collectors to improve the conversion efficiency, nano-antennas must cover the broad spectrum of incident solar radiation [6–8].

As tightly localized broadband optical sources can be employed for spectroscopy, multiplexed sensors and polarization division [9,10], many broadband nano-antennas have been proposed. For example, Kotter et al. [7] employed broadband spiral nano-antennas as solar nano-antenna electromagnetic collectors (NECs). Based on the theory of scaling a radio-frequency antenna to the infrared and visible regions, these devices were designed to target mid-infrared wavelengths where there is an abundance of solar energy but conventional photovoltaic (PV) solar cells are inefficient [7]. Boriskina and Dal Negro [11] presented grating-assisted nano-antennas that provide multi-wavelength focusing in a single sub-wavelength spot by tuning the periodicities of the multiple-periodic gratings and particle radii. In addition, cross-dipole antennas have been used to obtain localized fields of various polarizations [12] while six-particle and eight-particle common-gap plasmonic nano-antennas with adjustable spectral responses have been demonstrated by Ünlü et al. [8].

---

*Corresponding author. Email: h.hattori@adfa.edu.au

In this research, a Charnia-like plasmonic nano-antenna device is studied [13]. Charnias were Ediacaran primitive life-forms that lived in the deep seas and exhibited a quasi-fractal growth pattern that was used for filter-feeding purposes. We study the effects of such a structure on the excitation of plasmonic waves. It has the potential to provide broadband plasmonic excitation. Finally, we experimentally investigate how this structure affects the Raman spectrum of ethanol by demonstrating a large SERS enhancement factor (EF).

SERS is a spectroscopic technique that can strongly enhance Raman signals when molecules are attached to modified gold or silver structures [14]. Since the discovery of SERS, the enhancement mechanisms are considered to be due to a combined enhancement effect of electric field, chemical and photonic density of states [15,16]. However, it is generally believed that the electromagnetic enhancement effect plays the dominant role. The stronger SERS due to electromagnetic field enhancement is due to the generation of strong localized surface plasmon resonances (LSPRs) on both the incident and Raman scattered waves [17,18]. The theoretical SERS enhancement factor (EF_{SERS}) can be calculated by,

$$EF_{SERS} \propto \frac{|E_{loc}(\omega_{ex})|^2}{|E_0(\omega_{ex})|^2} \frac{|E_{loc}(\omega_s)|^2}{|E_0(\omega_s)|^2}, \quad (1)$$

where $|E_{loc}(\omega_{ex})|$ is the amplitude of the enhanced local electric field at the incident frequency, $|E_0(\omega_{ex})|$ is the amplitude of the incident electric field at the incident frequency, $|E_{loc}(\omega_s)|$ is the amplitude of the enhanced local electric field at the Raman scattered frequency, and $|E_0(\omega_s)|$ is the amplitude of the incident electric field at the Raman scattered frequency.

2. General device designs and theoretical analysis

Based upon the skeletal structure of a Charnia, we created a plasmonic nano-antenna, as shown in Figure 1. This structure presents self-similarity properties, meaning that the structure at the arms resembles the main structure. However, the scaling factor of the secondary structure is not constant since the structure is optimized to produce a high electric field over a large range of frequencies. The structure shown in Figure 1 is made of gold on top of a quartz substrate. A titanium adhesion layer of 5 nm is added between gold and quartz to improve the adhesion of the gold layer to quartz. The thickness of the gold layer is $H = 300$ nm.

In order to analyze these devices, commercial three-dimensional finite difference time domain (FDTD) software [19] is employed. The polarization is set to be TE mode with main component of the magnetic field along the y-direction (H_y), perpendicular to the plane of
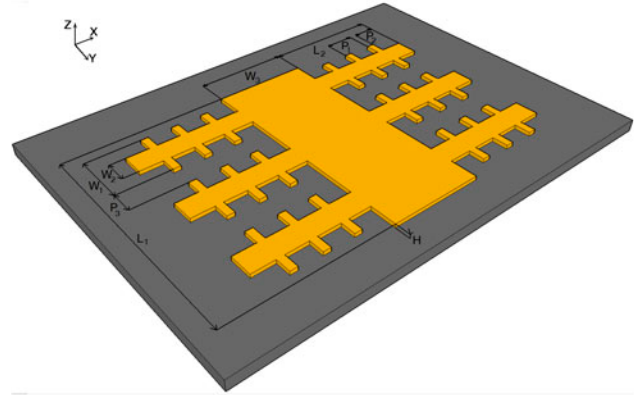
Figure 1. Schematic of a Charnia-like structure. (The colour version of this figure is included in the online version of the journal.)

the device [20]. The computational region is terminated by perfectly matched absorbing layers. The grid size specified in the calculations is non-uniform, being refined at the boundaries between the metallic and dielectric regions, where $\Delta x = \Delta y = \Delta z = 20$ nm but, close to the metallic regions, $\Delta x = \Delta y = \Delta z = 3$ nm. The time step is chosen as $\Delta t = 6.7 \times 10^{-18}$ s to ensure that the FDTD simulations are stable. Gold is assumed to be a very dispersive material with losses and material dispersion parameters are defined internally by the software [19].

In this section, the Charnia-like structure is designed to operate at the central free-space wavelength (λ) of 830 nm. A laser operating at this wavelength is available for the experiments. After optimizing different dimensions of the device to provide high electric field over a wide range of wavelengths centered around 830 nm, the following parameters are obtained: $L_1 = 7300$ nm, $L_2 = 3220$ nm, $P_1 = 870$ nm, $P_2 = 610$ nm, $P_3 = 660$ nm, $W_1 = 1540$ nm, $W_2 = 660$ nm, $W_3 = 2430$ nm, and $H = 300$ nm. In the simulations, a uniform plane wave coming from the vertical (y) direction is incident on the computational area with spot size diameter of 10 μm.

The electric field EF (η_{enh}) is defined as the ratio between the electric field at the surface of the nano-antenna gap (E_{nano}) and the electric field of the incident wave (E_{inc}),

$$\eta_{enh} = \frac{E_{nano}}{E_{inc}}. \quad (2)$$

Since the field distribution along the nano-antenna is usually non-uniform, with stronger fields close to the edges of the dipole arms, we consider E_{nano} as being the electric field in the middle of the air gap in the arms of the fractal structure. In the structure in Figure 1, the electric field enhancement is nearly constant and equal to 8.8 in the wavelength region between 800 nm and 900 nm,

Z. Li et al.
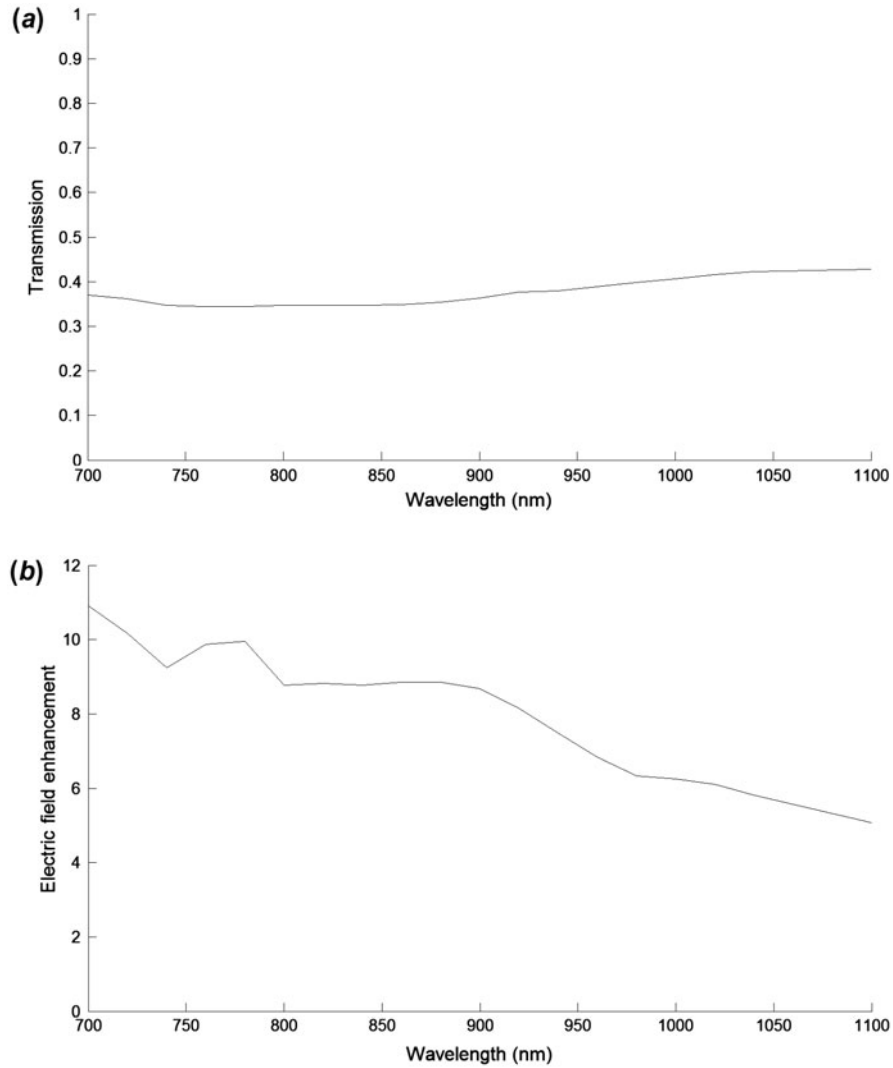
Figure 2. (*a*) Transmission spectrum and (*b*) electric field enhancement as function of wavelength for Charnia-like structure.

above 8.8 for 700 nm $< \lambda <$ 800 nm and starts to decrease for $\lambda >$ 900 nm.

Figure 2 shows the theoretical transmission spectrum and electric field enhancement as a function of free-space wavelength (λ) for the device. In the wavelength range between 700 nm and 1100 nm, the transmission efficiency changes by only 14% while the average transmission through the structure is 45%. The electric field distribution profiles at 700 nm, 800 nm, 900 nm, and 1000 nm are shown in Figure 3 and in which different hot-spot regions can be identified. In the wavelength range close to 700 nm, a strong electric field is generated along the *z*-direction while, at wavelengths close to 1000 nm, there are strong resonances along the *x*-direction. Although the resonances along the *z*-direction are still strong at wavelengths close to 1000 nm, the electric field enhancement drops because this modified structure is not designed to work beyond 1000 nm.

3. Fabrication and experimental results

Initially, a 5 nm-thick layer of titanium is deposited on top of a quartz substrate followed by a deposition of 150 nm of gold. After depositing these metallic films, the structure is created by patterning its gold elements using a FEI Hellios NanoLab 600 dual-beam focused ion beam (FIB) system. A tightly focused Ga+ ion with energy of 30 keV and a beam current of 9.7 pA is used for FIB milling. In Figure 4, the light gray areas represent the regions covered with Ti/Au layers.

To measure the resonance spectra of fabricated plasmonic structure, white light transmission micro-absorption is used. Figure 4 shows the transmission spectrum for the Charnia-like structure, which cover surfaces of 11 $\times$ 11 μm^2, while the spot-size diameter of the incident beam is about 25 μm. Since the light from an incident beam with such a large spot-size diameter will impinge on regions that are not part of our structure by
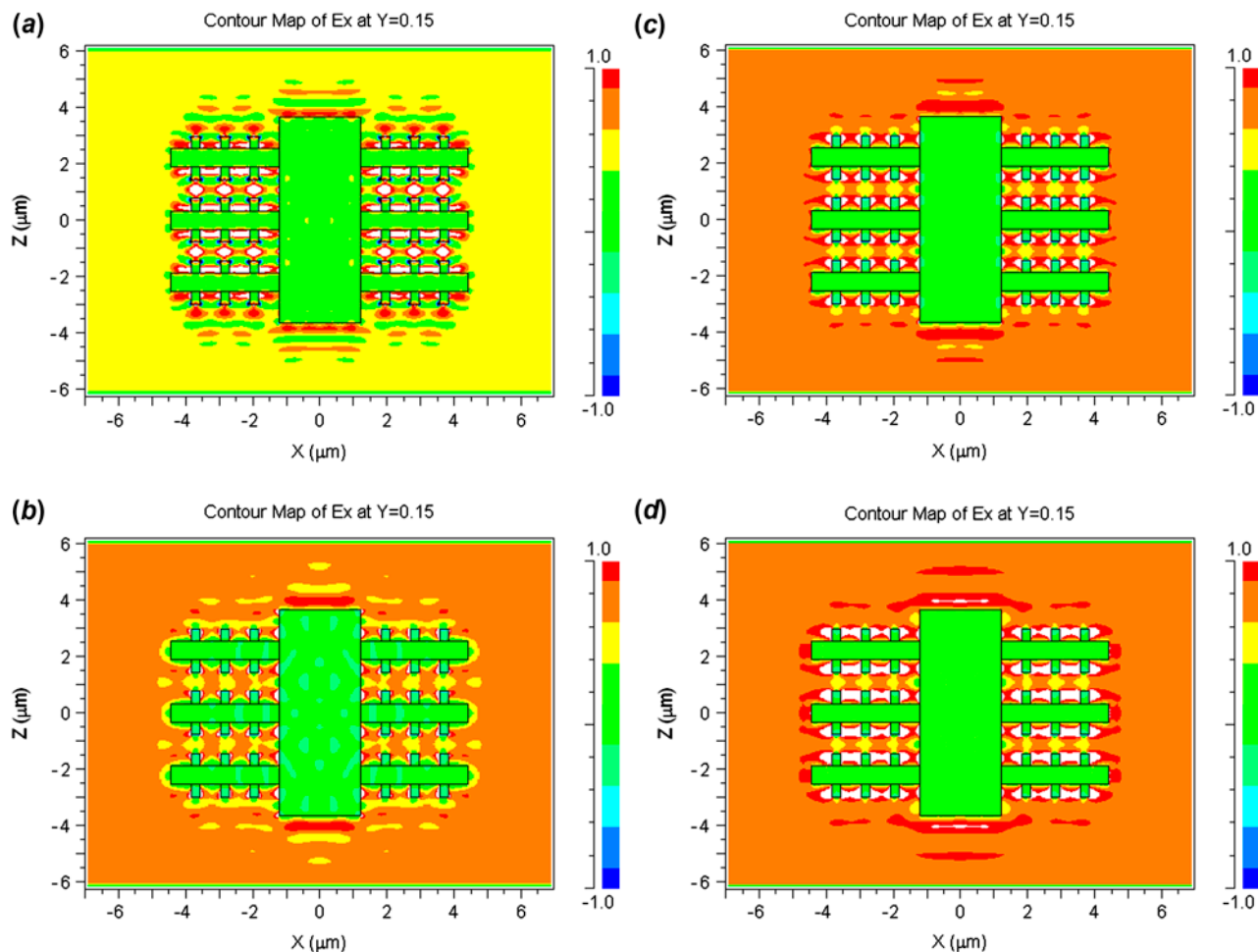
Figure 3. Electric field distribution profiles of wavelengths at (*a*) 700 nm, (*b*) 800 nm, (*c*) 900 nm, and (*d*) 1000 nm. (The colour version of this figure is included in the online version of the journal.)

the FIB, i.e. metallic Au regions, and block the light, we multiply the actual transmission by an area factor to take into account this blocking effect and amend the plots in Figure 5. For the Charnia-like structure, similar to the calculation results, the experimental transmissions change very little in the wavelength range between 700 nm and 1100 nm, but the efficiency is slightly reduced, from 60% to 50%. We have extra 'stubborn' metallic grains, as shown in Figure 4, due to the channeling effect based on the crystallographic orientation of the grains during FIB milling [21,22], thus, we may have a greater scattering of light in this structure.

In principle, the large electric field enhancement could be used to measure SERS at different wavelengths. In fact, an array of similar Charnia-like plasmonic devices could be fabricated in different parts of a large material and different parts of the material could be excited by lasers operating at distinct wavelengths. Based upon the Raman spectra produced at different regions of the material, information about variations in material density and presence of contaminants in the material
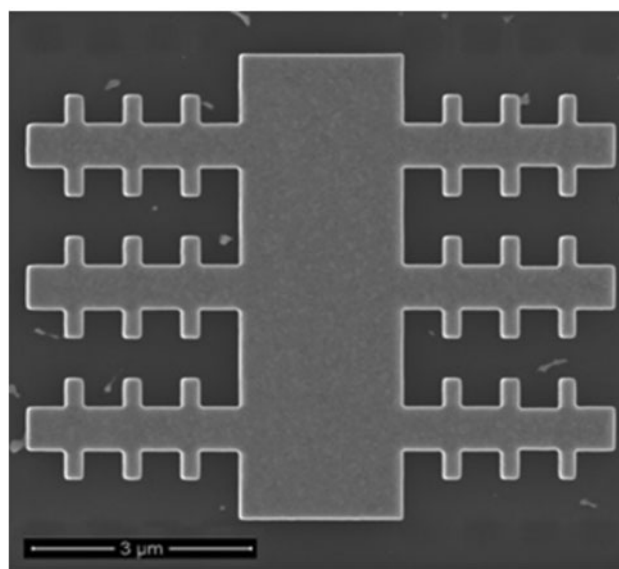
Figure 4. Scanning electron microscope (SEM) image of Charnia-like structure.
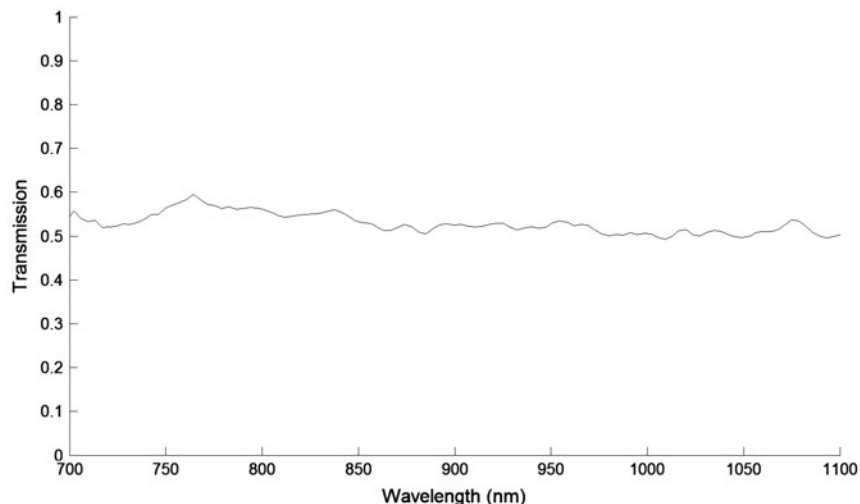
Figure 5.   Transmission spectrum of Charnia-like structure.

could be detected by this array of Charnia nano-antennas. In order to assess the potential of this structure to enhance SERS spectra, SERS spectra for 100% ethanol with a concentration of approximately 17 mol/l were measured. A laser diode working at 830 nm and polarized along the x-direction is focused on the samples using a 50× objective lens (numerical aperture (NA) of 0.55) with a spot-size diameter close to 5 μm from the vertical direction. Laser power is about 14 mW. After the solution is dropped on the surface of the sample, it is bound to the surface by a very thin glass slide placed on top of it. In this way, we ensure that the molecules of ethanol attach well to the surface of the device at a uniform height. The Raman intensities, averaged over five spectra for each structure with acquisition times of 60 s, are compared with those of a reference quartz surface under the same conditions measured by a confocal Micro-Raman system (Horiba Jobin Yvon 64000). The schematic of this Raman confocal measurement system is shown in Figure 6(*a*). As clearly shown in Figure 6(*b*), strong and sharp Raman shifts are present at 880 cm^{-1}, which is the characteristic Raman shift for ethanol [23].

The experimentally measured SERS enhancement factor is given by [16,24–26],

$$EF_{SERS} = \frac{I_{SERS}/N_{surf}}{I_{ref}/N_{bulk}}, \qquad (3)$$

where I_{SERS} is the SERS intensity, N_{surf} is the number of molecules on the structured substrates, I_{ref} is the Raman intensity from the reference region, N_{bulk} is the number of molecules within the excitation volume of the laser spot for the analyte in the reference region. N_{surf} can be calculated as

$$N_{surf} = \mu s AM, \qquad (4)$$

where μ_S is the surface packing density of the analyte on gold, A_M is the surface area of the pattern (top and outer wall surfaces), and N_{bulk} can be calculated by

$$N_{bulk} = C_{RS} N_A H_{eff} A_{laser}, \qquad (5)$$

where C_{RS} is the concentration of the solution used for the non-SERS measurement, N_A is the Avogadro's number, H_{eff} is a parameter defined by the confocal volume
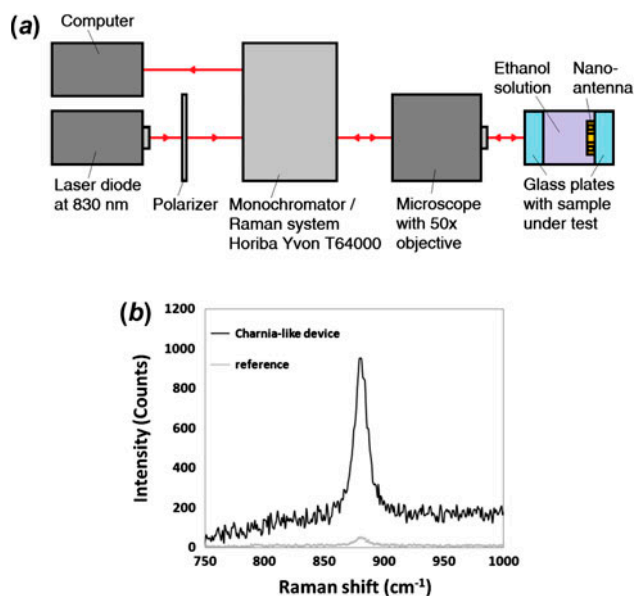
Figure 6.   (*a*) Schematic of the measurement setup. (*b*) Raman spectra of Charnia-like device with quartz surface as reference. (The colour version of this figure is included in the online version of the journal.)

Table 1. Typical parameters.

Symbol	Quantity	Typical value
μ_s	Surface-packing density of 100% ethanol on gold	9.88×10^{18} m^{-2}
C_{RS}	Concentration of solution used for non-SERS measurement	1.71×10^4 mol/m^3
N_A	Avogadro's number	6.02×10^{23} mol^{-1}
H_{eff}	Parameter defined by confocal volume of spectrometer (measured experimentally in our setup)	2.93×10^{-5} m

of the spectrometer, A_{laser} is the excitation laser spot size area at 2.83×10^{-11} m^2 and $A_M = 6.15 \times 10^{-11}$ m^{-2}. Typical values of these parameters are summarized in Table 1. From these equations, a SERS enhancement factor of 2.56×10^5 is obtained for the 880 cm^{-1} line of ethanol, which is close to the values recently obtained by other researchers [27]. In terms of SERS enhancement factors (EF_{SERS}), some plasmonic nanostructures can produce higher EF_{SERS}: for example, metal coated nanodomes [15], plasmonic nanorings [24] and staircase nano-antennas [28] have EF_{SERS} in the order of 3×10^6, 4×10^6 and 2.4×10^6, respectively, but they operate over a narrow bandwidth. In terms of bandwidth, Kotter et al. [7] have designed a nano-antenna with a bandwidth of 2 μm but operating at the wavelength of 10 μm (20% bandwidth), while Ünlü et al. [8] designed structures with bandwidths between 340 nm to 990 nm – our nano-antenna can produce large enhancement of electric field over a bandwidth above 200 nm. On the other hand, the six-particle and eight-particle nano-antennas [8] were not fabricated, while the presented nano-antenna has a high level of manufacturing tolerance and may be even fabricated by using deep-UV lithography.

4. Conclusions

A Charnia-like plasmonic nano-antenna has been analyzed theoretically and experimentally. It is shown that the device can provide electric field enhancement above 8.8 in the wavelength range from 700 nm to 900 nm. A SERS enhancement factor of 2.56×10^5 is obtained for the 880 cm^{-1} line of ethanol, indicating a potential application of this nano-antenna. It could also find applications in sensing, particle manipulation, and nano-imaging. Moreover, taking into account their large bandwidths, they could work as a single sensor in a wavelength division multiplexed sensing system and, potentially, undertake imaging of nanoparticles over a wide range of wavelengths.

Acknowledgements

References

[1] Bharadwaj, P.; Deutsch, B.; Novotny, L. *Adv. Opt. Photonics* **2009,** *1,* 438–483.
[2] Novotny, L.; Van Hulst, N. *Nat. Photonics* **2011,** *5,* 83–90.
[3] Fischer, H.; Martin, O.J.F. *Opt. Express* **2008,** *16,* 9144–9154.
[4] Yu, N.F.; Cubukcu, E.; Diehl, L.; Bour, D.; Corzine, S.; Zhu, J.T.; Höfler, G.; Crozier, K.B.; Capasso, F. *Opt. Express* **2007,** *15,* 13272–13281.
[5] Yu, N.; Cubukcu, E.; Diehl, L.; Belkin, M.A.; Crozier, K. B.; Capasso, F.; Bour, D.; Corzine, S.; Höfler, G. *Appl. Phys. Lett.* **2007,** *91,* 173113.
[6] Green, M.A.; Pillai, S. *Nat. Photonics* **2012,** *6,* 130–132.
[7] Kotter, D.K.; Novack, S.D.; Slafer, W.D.; Pinhero, P.J. *J. Sol. Energy Eng.* **2010,** *132,* 011014.
[8] Ünlü, E.S.; Tok, R.U.; Sendur, K. *Opt. Express* **2011,** *19,* 1000–1006.
[9] Bakker, R.M.; Drachev, V.P.; Yuan, H.K.; Shalaev, V.M. *Phys. B (Amsterdam, Neth.)* **2007,** *394*, 137–140.
[10] Simón, J.; Gonzalez, F.J. *Electron. Lett.* **2011,** *47,* 120–121.
[11] Boriskina, S.V.; Dal Negro, L. *Opt. Lett.* **2010,** *35,* 538–540.
[12] Biagioni, P.; Huang, J.S.; Duo, L.; Finazzi, M.; Hecht, B. *Phys. Rev. Lett.* **2009,** *102,* 256801.
[13] Li, Z.; Hattori, H.T.; Parkinson, P.; Tian, J.; Fu, L.; Tan, H.H.; Jagadish, C. Charnia-like Plasmonic Structure as a Surface Enhanced Raman Scattering Sensor. Presented at the International Conference on Nanoscience and Nanotechnology (ICONN), Perth, Australia, February 5–9, 2012; Paper 255.
[14] Kneipp, K.; Kneipp, H.; Itzkan, I.; Dasari, R.R.; Feld, M. S. *J. Phys.: Condens. Matter* **2002,** *14,* R597–R624.
[15] Choi, C.J.; Xu, Z.D.; Wu, H.Y.; Liu, G.L.; Cunningham, B.T. *Nanotechnology* **2010,** *21,* 415301.
[16] Le Ru, E.C.; Blackie, E.; Meyer, M.; Etchegoin, P.G. *J. Phys. Chem. C* **2007,** *111,* 13794–13803.
[17] Maier, S.A. *Plasmonics: Fundamentals and Applications*; Springer: New York, 2007.
[18] Shalaev, V.M.; Kawata, S. *Nanophotonics with Surface Plasmons*; Elsevier Science: Oxford, 2007.
[19] *Fullwave*, version 8.3; RSOFT Design Group: 2011.
[20] Hattori, H.T. *Appl. Opt.* **2008,** *47,* 2178–2185.
[21] Griswold, E.M.; Sharma, U.; Phaneuf, M.W. *J. Vac. Sci. Technol., A* **2004,** *22*, 930–934.
[22] Phaneuf, M.; Li, J.; Casey, J. Jr. *Microsc. Microanal.* **2002,** *8,* 52–53.

[23] Ashok, P.C.; Singh, G.P.; Tan, K.M.; Dholakia, K. *Opt. Express* **2010**, *18*, 7642–7649.

[24] Banaee, M.G.; Crozier, K.B. *Opt. Lett.* **2010**, *35*, 760–762.

[25] Cai, W.B.; Ren, B.; Li, X.Q.; She, C.X.; Liu, F.M.; Cai, X.W.; Tian, Z.Q. *Surf. Sci.* **1998**, *406*, 9–22.

[26] Cintra, S.; Abdelsalam, M.E.; Bartlett, P.N.; Baumberg, J.J.; Kelf, T.A.; Sugawara, Y.; Russel, A.E. *Faraday Discuss.* **2006**, *132*, 191–199.

[27] Lin, C.H.; Jiang, L.; Zhou, J.; Xiao, H.; Chen, S.J.; Tsai, H.L. *Opt. Lett.* **2010**, *35*, 941–943.

[28] Li, Z.; Hattori, H.T.; Parkinson, P.; Tian, J.; Fu, L.; Tan, H. H.; Jagadish, C. *J. Phys. D: Appl. Phys.* **2012**, *45*, 305102.